J. Fluid Mech. (1992), vol. 241, pp. 145–168
Printed in Great Britain

A comparison of the solutions of some proposed equations of motion of granular materials for fully developed flow down inclined planes

By K. G. ANDERSON AND R. JACKSON
Department of Chemical Engineering, Princeton University, Princeton, NJ 08544, USA

(Received 19 August 1991 and in revised form 20 January 1992)

In the past few years kinetic theory has been used to derive equations of motion for rapidly shearing granular materials, and there have been empirical extensions of these to take into account stress transmitted by sustained sliding and rolling contacts between particles. The equations are complicated and solutions have been generated only for very simple flows. In this paper three forms for the equations of motion are considered; one representing interaction by collisions only, one which is a high-density asymptotic form of this, and a third which includes terms representing the 'frictional' stresses associated with the sustained contacts referred to above. Solutions are found for fully developed flow under gravity down an inclined plane, and it is shown that the relation between the flow rate and the depth of the flowing layer predicted by the first two sets of equations is not in accord with observations. The third form appears to eliminate much of the discrepancy, but its predictions have not been explored over the whole parameter space. It is emphasized that the form of the solutions should be studied over a wide range of operating conditions in order to assess the usefulness of proposed equations.

1. Introduction

In recent years a great deal of work has been devoted to the development of equations of motion for rapidly deforming granular materials, using the methods of kinetic theory (see, for example, the extensive review by Campbell 1990), but much less effort has been devoted to solving the resulting equations of motion and examining the solutions, over wide ranges of conditions, in relation to experimental evidence and intuitive expectations. Some solutions that have been published either do not correspond to any physically realizable situation (for example, uniform plane shear), or they invoke simplifications of the equations, or boundary conditions which are unlikely to be justified. Others represent complete solutions, but have been computed for only one, or a small set of parameter values or operating conditions. For various equations of motion that have been proposed it would, therefore, be valuable to generate solutions representing measurable responses of some real experimental apparatus over a wide range of operating conditions, so as to assess whether the equations are at least able to predict a reasonably correct *pattern* of behaviour.

This is the objective of the present work, the apparatus in question being an inclined plane down which a layer of granular material flows under gravity. Solutions for fully developed flow will be obtained for three different sets of equations of motion. The first is the set of equations obtained by a formal application of the

methods of kinetic theory to a granular material whose grains interact entirely through slightly inelastic collisions. The form of these equations is by now well established, with only minor differences remaining between different authors. (To be specific, we use the equations of Lun *et al.* 1984.) The second is an earlier set of equations derived by Haff (1983) using heuristic arguments, again based in kinetic theory but appropriate only at high concentrations. With a suitable choice of certain undetermined parameters in these equations they can be made to match the high-density limit of the equations of Lun *et al.* The third set of equations studied is an extension of those of Lun *et al.* to account, rather crudely, for the fact that particles can also interact by forces transmitted at points of sustained sliding or rolling contact. This mechanism of stress transmission is modelled simply by adding extra terms to the stress tensor to represent a Coulomb material; a device originally introduced by Savage (1983) and later used by Johnson & Jackson (1987) in studies of plane shear in a horizontal layer, and by Johnson, Nott & Jackson (1990) for flow down an inclined plane.

It will be shown that the purely collisional theories (i.e. the first and second above) lead to relations between the depth of the flowing layer and the flow rate which appear to be unrealistic, based on the experimental evidence presently available, while the additional terms introduced in the third theory seem able to overcome this difficulty.

2. Equations of motion

There are three equations of motion, which take the following form. First a continuity equation

$$\frac{\mathrm{D}\rho}{\mathrm{D}t}+\rho\nabla\cdot\boldsymbol{u}=0, \tag{1}$$

where ρ is the bulk density and $\boldsymbol{u}$ the velocity of the flowing material. Second a momentum balance

$$\rho\frac{\mathrm{D}\boldsymbol{u}}{\mathrm{D}t}=\rho\boldsymbol{g}-\nabla\cdot\boldsymbol{\sigma}, \tag{2}$$

where $\boldsymbol{g}$ is the specific gravity force and $\boldsymbol{\sigma}$ denotes the stress tensor. Finally, a balance on the pseudo-thermal energy of random motion of the particles, which takes the form

$$\tfrac{3}{2}\rho\frac{\mathrm{D}T}{\mathrm{D}t}=-\nabla\cdot\boldsymbol{q}_{\mathrm{PT}}-\boldsymbol{\sigma}:\nabla\boldsymbol{u}-I. \tag{3}$$

Here T denotes the 'particle temperature', $T=\frac{1}{3}v^2$, where v^2 is the mean-square speed of the fluctuating component of the particle velocity, $\boldsymbol{q}_{\mathrm{PT}}$ is the flux vector of pseudo-thermal energy, and I is the rate of dissipation of pseudo-thermal energy by inelastic collisions, per unit total volume. In all the above equations $\mathrm{D}/\mathrm{D}t$ denotes the substantial derivative following the particle motion. The second term on the right-hand side of (3) represents the rate of generation of pseudo-thermal energy by working of the stress.

The literature contains a number of closures of these equations derived using the methods of the kinetic theory of dense gases. In earlier publications (Johnson & Jackson 1987; Johnson *et al.* 1990) we have used a slightly modified form of the closure of Lun *et al.* (1984), and for consistency this will be retained in the present

work. The stress is then written as the sum of collisional and kinetic contributions, $\boldsymbol{\sigma} = \boldsymbol{\sigma}_c + \boldsymbol{\sigma}_k$, where

$$\boldsymbol{\sigma}_c = 4\rho_p T\eta\nu^2 g_0 \boldsymbol{I} - \frac{64\mu\nu}{15(2-\eta)}[1+\tfrac{8}{5}\eta(3\eta-2)\nu g_0]\boldsymbol{S} - \eta\mu_b[\tfrac{24}{15}\boldsymbol{S} + (\boldsymbol{\nabla}\cdot\boldsymbol{u})\boldsymbol{I}] \tag{4}$$

and

$$\boldsymbol{\sigma}_k = \rho_p \nu T\boldsymbol{I} - \frac{8\mu}{3\eta(2-\eta)g_0}[1+\tfrac{8}{5}\eta(3\eta-2)\nu g_0]\boldsymbol{S}. \tag{5}$$

Here $\boldsymbol{S}$ is the deviatoric part of the rate of deformation tensor for the velocity field $\boldsymbol{u}$ and $\boldsymbol{I}$ denotes the unit tensor. Also ρ_p is the intrinsic density of the particles, ν is the solids volume fraction, and $\eta = \frac{1}{2}(1+e)$, where e is the coefficient of restitution for collisions between pairs of particles. g_0 is the radial distribution function, whose form is defined below, while μ and μ_b are the effective shear and bulk viscosities for perfectly elastic particles, given by

$$\mu = \frac{5m(T/\pi)^{\frac{1}{2}}}{16d^2}, \quad \mu_b = \frac{256\mu\nu^2 g_0}{5\pi},$$

where m and d are the mass and diameter of a particle, respectively. The collisional and kinetic contributions to $\boldsymbol{q}_{PT}$ are

$$\boldsymbol{q}_c = -\frac{12\eta\lambda_1\nu}{5}\left\{[1+\tfrac{12}{5}\eta^2(4\eta-3)\nu g_0 + \tfrac{16}{15\pi}(41-33\eta)\eta\nu g_0]\boldsymbol{\nabla}T + \frac{12}{5}\eta(2\eta-1)(\eta-1)\frac{\mathrm{d}}{\mathrm{d}\nu}(\nu^2 g_0)\frac{T}{\nu}\boldsymbol{\nabla}\nu\right\} \tag{6}$$

and

$$\boldsymbol{q}_k = -\frac{\lambda_1}{g_0}\left\{[1+\tfrac{12}{5}\eta^2(4\eta-3)\nu g_0]\boldsymbol{\nabla}T + \tfrac{12}{5}\eta(2\eta-1)(\eta-1)\frac{\mathrm{d}}{\mathrm{d}\nu}(\nu^2 g_0)\frac{T}{\nu}\boldsymbol{\nabla}\nu\right\}, \tag{7}$$

where λ is the thermal conductivity for elastic particles at low concentration and λ_1 is the thermal conductivity for inelastic particles, given by

$$\lambda = \frac{75m(T/\pi)^{\frac{1}{2}}}{64d^2}, \quad \lambda_1 = \frac{8\lambda}{\eta(41-33\eta)}.$$

Finally, the rate of dissipation of pseudo-thermal energy, per unit volume, is given by

$$I = \frac{48}{\pi^{\frac{1}{2}}}\eta(1-\eta)\frac{\rho_p\nu^2}{d}g_0 T^{\frac{3}{2}}. \tag{8}$$

In the above equations the radial distribution function is taken to be

$$g_0 = \frac{1}{1-(\nu/\nu_0)^{\frac{1}{3}}},$$

which diverges as the volume fraction approaches its maximum value ν_0, thus ensuring that the stress also diverges in these circumstances.

The above constitutive relations are valid only when the coefficient of restitution e, and consequently also η, takes a value close to unity. Then it is found that η can be replaced by unity everywhere except in the term $1-\eta$ in (8), thus simplifying the algebra without significant effect on most of the computed results.

An alternative set of constitutive relations, based on kinetic theory but valid only for volume fractions near ν_0, was derived by Haff (1983) using heuristic arguments. These take the following form:

$$\boldsymbol{\sigma} = \frac{t\rho d v^2}{s}\boldsymbol{I} - 2q\rho d^2 \frac{v}{s}\boldsymbol{S}, \tag{9}$$

$$\boldsymbol{q}_{\mathrm{PT}} = -\frac{r\rho d^2}{2}\frac{v}{s}\boldsymbol{\nabla}(v^2), \tag{10}$$

$$I = \gamma(1-e^2)\rho\frac{v^3}{s}, \tag{11}$$

where s is the mean separation between the surfaces of adjacent particles, t, q, r and γ are dimensionless constants of order unity, and it is convenient to write the relations in terms of v, the r.m.s. speed of velocity fluctuations, rather than the particle temperature T. Also, the bulk density ρ may be replaced by its maximum value ρ_0 wherever it appears in these equations. Small variations in density away from ρ_0 are then taken into account through the factor s. Haff's arguments do not give the values of t, q, r and λ, but it is easy to show that the constitutive relations of Lun *et al.*, given above, reduce to Haff's form in the limit as $\nu \to \nu_0$ if the following values are assigned:

$$t = \frac{4}{3}\nu_0, \quad q = \nu_0\left(\frac{\pi}{3}\right)^{\frac{1}{2}}\left(\frac{8}{45}+\frac{32}{15\pi}\right), \quad r = \nu_0\left(\frac{\pi}{3}\right)^{\frac{1}{2}}\left(\frac{3}{4}+\frac{8}{3\pi}\right), \quad \gamma = \frac{4}{(3\pi)^{\frac{1}{2}}}\nu_0. \tag{12}$$

Then the Haff closure becomes the high-density limit of the closure of Lun *et al.*

Both the above sets of constitutive relations are based on a physical picture of interactions between pairs of particles in which the time spent in contact is short compared with the time of free flight between collisions. However, as the volume fraction approaches ν_0 particles will, to an increasing extent, be in simultaneous contact with several neighbours, and stress will be transmitted by contact forces at points of sustained sliding and rolling contact. It is very difficult to treat this situation at the microscopic level, but several empirical constitutive relations are available in the literature of soil mechanics. In general they are quite complicated, but for plane shearing motion they all reduce to a proportionality between normal, N_{f}, and tangential, T_{f}, stresses on the planes of shear, together with an algebraic relation between the normal stress and the volume fraction of solids.

$$S_{\mathrm{f}} = N_{\mathrm{f}}\sin\phi, \quad N_{\mathrm{f}} = N_{\mathrm{f}}(\nu). \tag{13}$$

We might expect N_{f} to increase without bound when $\nu \to \nu_0$, and to become zero when ν is smaller than some limiting value $\nu_{\min}$, and Johnson *et al.* (1990) used an expression of the following form:

$$\begin{aligned} N_{\mathrm{f}}(\nu) &= Fr\frac{(\nu-\nu_{\min})^p}{(\nu_0-\nu)^n} \quad (\nu > \nu_{\min}) \\ &= 0 \qquad\qquad\qquad (\nu \leqslant \nu_{\min}), \end{aligned} \tag{14}$$

where Fr, n and p are constants.

The mechanism of stress generation is, in practice, intermediate between the two situations described above, and we presently have no method of treating this

theoretically. Following a suggestion of Savage (1983), Johnson *et al.* (1990) simply expressed the total stress as the sum of contributions from the separate mechanisms, each evaluated as though it acted alone. Thus

$$\boldsymbol{\sigma} = \boldsymbol{\sigma}_{\mathrm{k}} + \boldsymbol{\sigma}_{\mathrm{c}} + \boldsymbol{\sigma}_{\mathrm{f}},$$

where $\boldsymbol{\sigma}_{\mathrm{c}}$ and $\boldsymbol{\sigma}_{\mathrm{k}}$ are given by (4) and (5), respectively, while the tangential and normal components of $\boldsymbol{\sigma}_{\mathrm{f}}$ are given by (13) and (14) for plane shear. However, in the second term on the right-hand side of the pseudo-thermal energy balance (3) only the first two terms in the above expression for $\boldsymbol{\sigma}$ are retained, corresponding to an assumption that the contribution of rolling and sliding at multiple contacts to the random component of particle motion can be neglected.

Boundary conditions at a solid surface in contact with the shearing material can be found by writing balances of force and pseudo-thermal energy on a vanishingly thin layer of material adjacent to the wall. If $\boldsymbol{u}_{\mathrm{w}}$ is the velocity of the wall and $\boldsymbol{u}$ that of the material adjacent to the wall we define the slip velocity by $\boldsymbol{u}_{\mathrm{sl}} = \boldsymbol{u} - \boldsymbol{u}_{\mathrm{w}}$, and denote its magnitude by u_{sl}. We also define a unit vector $\boldsymbol{n}$, normal to the wall and pointing into the flowing material. The tangential stress in the material adjacent to the wall is in the direction of $\boldsymbol{u}_{\mathrm{sl}}$, and its magnitude will be denoted by S. Then a force balance on the above thin layer gives

$$S = c(\phi' m u_{\mathrm{sl}})\left(\frac{ndv}{s}\right) + N_{\mathrm{f}} \tan\delta. \tag{15}$$

The second term on the right-hand side represents the frictional stress between the wall and the granular material sliding over it, with δ denoting the angle of friction between the material and the wall. The first term represents the rate of transfer of tangential momentum to unit area of the wall by particles colliding with it. The first factor in brackets is proportional to the average momentum transferred in each collision, where m is the mass of a particle and ϕ' is a 'specularity factor', which measures the fraction of the momentum of the incident particle transferred to the wall. (ϕ' is zero for perfectly specular rebound and unity for diffuse scattering.) The second bracketed factor represents the number of collisions per unit time on unit area of the wall, and c is a dimensionless proportionality constant of order unity. Similarly, an energy balance gives

$$\boldsymbol{n}\cdot\boldsymbol{q}_{\mathrm{PT}} = c(\phi' m u_{\mathrm{sl}})\left(\frac{ndv}{s}\right) u_{\mathrm{sl}} - a(\tfrac{1}{2}mv^2)\,(1-e_{\mathrm{w}}^2)\left(\frac{ndv}{s}\right). \tag{16}$$

Here the first term on the right-hand side represents the rate of working of the forces exerted at the wall by the particles colliding with it, while the second term is the rate of dissipation of kinetic energy of particle velocity fluctuations because of the inelasticity of collisions with the wall. In this term the first factor in brackets is the average kinetic energy of an incident particle, the second is the fraction of this lost in the collision, with e_{w} denoting the coefficient of restitution for collisions with the wall, the third is the number of collisions per unit time, and a is a dimensionless proportionality constant of order unity. For a more complete analysis of the form of the boundary condition, see §2.2 of Johnson *et al.* (1990).

Since the closure relations of Haff ((9)–(11) above) are written in terms of v and s, boundary conditions in the form of (15) and (16) are directly suitable for use with equations of motion based on Haff's closure. The more complete closure relations of Lun *et al.* ((4)–(8)), on the other hand, are written in terms of the particle

temperature T and the volume fraction ν, so for use with them it is convenient to rewrite the boundary conditions in terms of these variables, using the relations

$$T = \tfrac{1}{3}v^2, \quad s/d = 1-(\nu/\nu_0)^{\frac{1}{3}},$$

the second of which is valid only when $s \ll d$. Thus (15) and (16) can be rewritten as

$$S = \frac{c\phi'\rho_p \nu u_{sl}(3T)^{\frac{1}{2}}}{1-(\nu/\nu_0)^{\frac{1}{3}}} + N_f \tan\delta \tag{17}$$

and

$$\boldsymbol{n}\cdot\boldsymbol{q}_{PT} = \frac{c\phi'\rho_p \nu u_{sl}^2(3T)^{\frac{1}{2}}}{1-(\nu/\nu_0)^{\frac{1}{3}}} - \frac{a}{2}\frac{\rho_p \nu(3T)^{\frac{3}{2}}(1-e_w^2)}{1-(\nu/\nu_0)^{\frac{1}{3}}}. \tag{18}$$

The values of the dimensionless factors a and c remain to be determined, and it is easy to show that the choice

$$a = c = \pi/6\nu_0 \tag{19}$$

makes (17) and (18) exactly equivalent to the boundary conditions used by Johnson *et al.* (1990).

We can now envisage three different theoretical approaches to the problem of fully developed flow down an inclined plane, namely:

(*a*) Equations (1)–(3), with $\boldsymbol{\sigma} = \boldsymbol{\sigma}_k + \boldsymbol{\sigma}_c$, and the closure of Lun *et al.* (1984), as embodied in (4)–(8), supplemented by the boundary conditions (17) and (18) (with $N_f = 0$) at the surface of the plane. Physically, this takes account of interactions between pairs of particles, and between particles and the surface of the inclined plane, only through the mechanism of almost elastic collisions, but it represents this mechanism correctly over the whole range of bulk densities.

(*b*) The limiting form of this theory for volume fractions near the maximum possible value, ν_0. The Haff closure ((9)–(11)) is then used, with the parameter values given in (12), and the boundary conditions at the surface of the inclined plane are (15) and (16), with $N_f = 0$.

(*c*) A theory which includes the effects of stress transmitted at sliding and rolling contacts. The stress tensor is then written $\boldsymbol{\sigma} = \boldsymbol{\sigma}_k + \boldsymbol{\sigma}_c + \boldsymbol{\sigma}_f$, where $\boldsymbol{\sigma}_f$ is introduced through equations (13) and (14), while $\boldsymbol{\sigma}_k$ and $\boldsymbol{\sigma}_c$ are obtained from the closure of Lun *et al.* The boundary conditions at the surface of the plane are (17) and (18), with N_f given by (14).

In what follows (*a*) will be referred to as the full collisional theory, (*b*) as the high-density collisional theory, and (*c*) as the frictional–collisional theory. We shall compare their predictions over a range of flow rates, at different inclinations, and with different roughnesses of the surface of the plane. Case (*b*) can be treated analytically, so we will start with that, then report numerical solutions for cases (*a*) and (*c*).

3. Solution for the high-density collisional theory

Figure 1 shows a layer of depth h in fully developed motion down a plane inclined at an angle θ to the horizontal; u denotes the velocity, which is directed parallel to the plane, and a coordinate z is measured in a direction normal to the plane from an origin in the free surface of the flowing layer. It is convenient to measure position from the surface, as it simplifies the solution of the high-density collisional theory. For the full frictional–collisional theory the coordinate is measured from the chute surface ($y = H - z$). Then if S and N denote the shear and normal stresses,

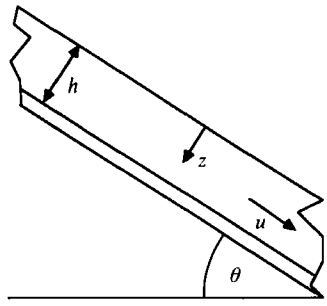

FIGURE 1. Notation for flow down an inclined plane.

respectively, on a plane of constant z, $S = \rho g z \sin\theta$ and $\mathrm{N} = \rho g z \cos\theta$ where, as before, ρ can be regarded as constant at its maximum value ρ_0. Using (9) to evaluate S and N these relation become

$$\rho g z \sin\theta = -qd^2\rho \frac{v}{s}\frac{\mathrm{d}u}{\mathrm{d}z}, \tag{20}$$

$$\rho g z \cos\theta = td\rho \frac{v^2}{s} \tag{21}$$

and, using (10) and (11) in the pseudo-thermal energy balance (3), we find

$$\frac{\mathrm{d}}{\mathrm{d}z}\left(rd^2\rho \frac{v^2}{s}\frac{\mathrm{d}v}{\mathrm{d}z}\right) - \rho g z \sin\theta \frac{\mathrm{d}u}{\mathrm{d}z} = \gamma(1-e^2)\frac{\rho v^3}{s}. \tag{22}$$

Dividing (20) by (21) gives

$$\frac{\mathrm{d}u}{\mathrm{d}z} = -\frac{t}{qd}\tan\theta\, v \tag{23}$$

and from (21)–(23) we find the following differential equation for v:

$$\frac{\mathrm{d}^2v}{\mathrm{d}z^2} + \frac{1}{z}\frac{\mathrm{d}v}{\mathrm{d}z} - \frac{(L - M\tan^2\theta)}{d^2}v = 0, \tag{24}$$

where

$$L = \frac{\gamma(1-e^2)}{r}, \quad M = \frac{t^2}{rq}. \tag{25}$$

When supplemented by suitable boundary conditions, equations (23) and (24) determine the profiles of velocity and particle temperature in the layer.

Setting $N_{\mathrm{f}} = 0$ the boundary condition (15) at the surface of the inclined plane can be written

$$\frac{\mathrm{d}u}{\mathrm{d}z} = -\frac{c\phi'}{qd}u \quad \text{at} \quad z = h \tag{26}$$

and, using (10), (23) and (26) the thermal boundary condition (16) can be reduced to

$$\frac{\mathrm{d}v}{\mathrm{d}z} = -(l - m\tan^2\theta)\frac{v}{d} \quad \text{at} \quad z = h, \tag{27}$$

$$l = \frac{a}{2r}(1 - e_{\mathrm{w}}^2), \quad m = \frac{t^2}{rc\phi'}. \tag{28}$$

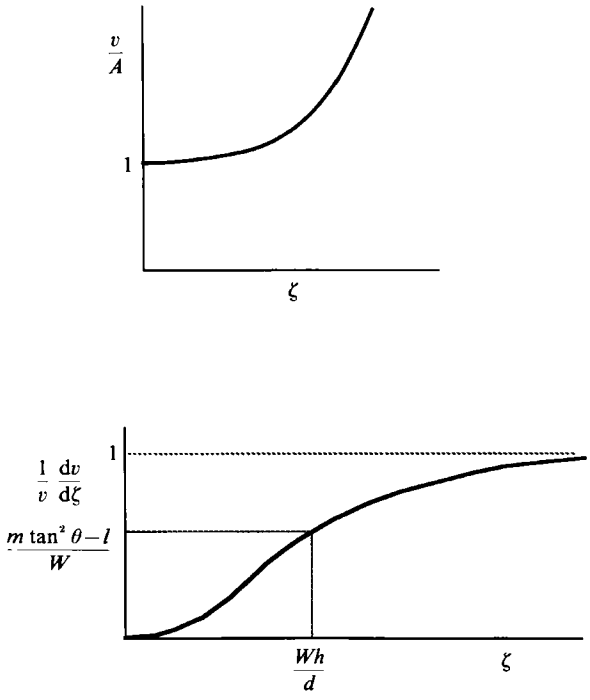

FIGURE 2. Illustration of the particle temperature profile and the thermal boundary condition for Case 1 of the high-density collisional theory.

At the free surface, $z = 0$, both the stress and the normal flux of pseudo-thermal energy must vanish, and these requirements complete the set of boundary conditions.

The form taken by the solution of (24) clearly depends on the sign of $L - M\tan^2\theta$, so there are two cases to consider.

Case 1: $L - M\tan^2\theta = W^2 > 0$.

Then, defining $\zeta = Wz/d$, (24) can be written

$$\frac{d^2v}{d\zeta^2} + \frac{1}{\zeta}\frac{dv}{d\zeta} - v = 0. \tag{29}$$

The relevant solution of this in the present case is $v = AI_0(\zeta)$, where I_0 is the modified Bessel function of order zero, since v must remain bounded as $\zeta \to 0$. Then it follows that $dv/d\zeta \to 0$ as $\zeta \to 0$, since $I_0'(0) = 0$. Thus the condition of vanishing pseudo-thermal energy flux is satisfied at the free surface.

The thermal boundary condition (27) can now be written as

$$\frac{1}{v}\frac{dv}{d\zeta} = \frac{m\tan^2\theta - l}{(L - M\tan^2\theta)^{\frac{1}{2}}} \quad \text{at} \quad \zeta = Wh/d, \tag{30}$$

and from figure 2 we see that (30) determines a unique value for h if, and only if,

$$0 < \frac{m\tan^2\theta - l}{(L - M\tan^2\theta)^{\frac{1}{2}}} < 1.$$

Since the denominator is positive, these inequalities require that

$$\frac{l}{m} < \tan^2\theta < \tan^2\theta_0 \left(< \frac{L}{M} \right), \tag{31}$$

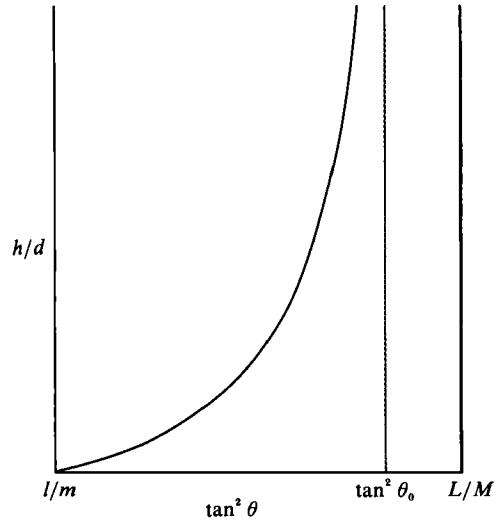

FIGURE 3. Dependence of the depth of the flowing layer on the inclination of the plane for Case 1 of the high-density collisional theory.

where

$$m\tan^2\theta_0 - 1 = (L - M\tan^2\theta_0)^{\frac{1}{2}}. \tag{32}$$

From figure 2 we see that the depth h of the flowing layer increases monotonically with increasing θ, and tends to infinity as $\theta \to \theta_0$, as sketched in figure 3.

The behaviour of this solution is rather odd. The depth of the flowing layer depends only on the inclination of the plane and, in particular, it is independent of the flow rate of the granular material. Furthermore, the depth increases as the inclination increases, which is contrary to the intuitive idea that the layer should become shallower and the velocity greater at larger inclinations. The particle temperature increases monotonically on moving down through the layer from the free surface.

The velocity profile is obtained by substituting the solution for v into (23), integrating, and invoking the slip boundary condition (26), with the result

$$u(z) = A\frac{t\tan\theta}{qd}\left\{\int_z^h I_0(W\xi/d)\,\mathrm{d}\xi + \frac{qd}{c\phi'}I_0(Wh/d)\right\}. \tag{33}$$

Since h is determined by the inclination of the plane, the velocity profiles for all flow rates are similar at a given inclination, differing from each other only by the factor of proportionality A.

The bulk density of the material is found from s, which is determined as a function of z by equation (21). Since $v \to A$ when $z \to 0$, it follows that $s \to \infty$ at the surface of the flowing material, and this corresponds to zero bulk density. But the constitutive relations are valid only at high bulk density, so the solution is not consistent with the physical assumptions on which it is based, at least in some domain adjacent to the surface. It is easily checked that the tangential stress vanishes at this surface, as it should.

Note that there are no solutions for inclinations such that

$$\tan^2\theta_0 < \tan^2\theta < L/M$$

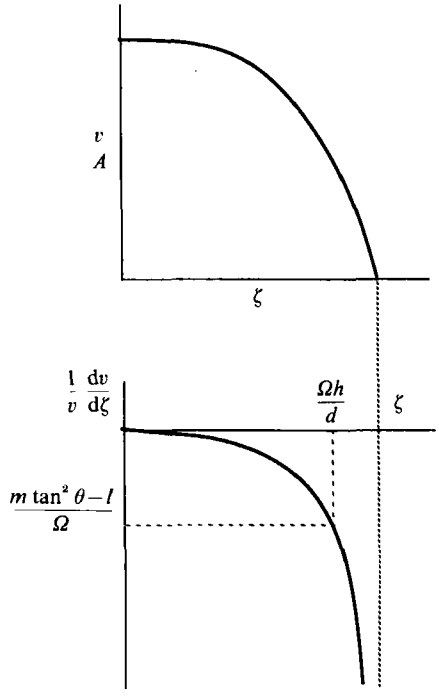

FIGURE 4. Illustration of the particle temperature profile and the thermal boundary condition for Case 2 of the high-density collisional theory.

though, as we shall see, solutions do exist for the full collisional theory in these circumstances.

Case 2: $L - M\tan^2\theta = -\Omega^2 < 0$.

Defining $\zeta = \Omega z/d$ in this case, (24) becomes

$$\frac{\mathrm{d}^2 v}{\mathrm{d}\zeta^2} + \frac{1}{\zeta}\frac{\mathrm{d}v}{\mathrm{d}\zeta} + v = 0 \tag{34}$$

and the solution which remains bounded as $\zeta \to 0$ is $v = AJ_0(\zeta)$. The thermal boundary condition (27) can now be written

$$\frac{1}{v}\frac{\mathrm{d}v}{\mathrm{d}\zeta} = \frac{m\tan^2\theta - l}{(M\tan^2\theta - L)^{\frac{1}{2}}}$$

and from figure 4 we see that this determines a unique value of h if, and only if,

$$\frac{m\tan^2\theta - l}{(M\tan^2\theta - L)^{\frac{1}{2}}} < 0.$$

Thus, solutions of this sort exist when

$$\frac{L}{M} < \tan^2\theta < \frac{l}{m} \tag{35}$$

and in this case there is no more-restrictive constraint like (32). From figure 4 we see that the depth of the flowing layer increases monotonically with decreasing θ, and tends to infinity as $\tan^2\theta \to L/M$ from above, as sketched in figure 5. This is more

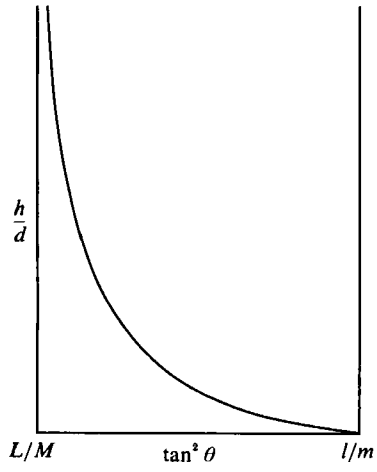

FIGURE 5. Dependence of the depth of the flowing layer on the inclination of the plane for Case 2 of the high-density collisional theory.

appealing to the intuition than the behaviour found in Case 1 above, though the depth of the layer is still determined entirely by θ, and is independent of the flow rate. ζ is constrained to remain smaller than the first zero of J_0, or the solution would contain intervals of negative v, which are physically meaningless. Also, in the present case the particle temperature decreases monotonically on moving down through the flowing layer.

In the same way as (33) was obtained for Case 1, the velocity profile in this case is given by

$$u(z) = A\frac{t\tan\theta}{qd}\left\{\int_z^h J_0(\Omega\xi/d)\,\mathrm{d}\xi + \frac{qd}{c\phi'}J_0(\Omega h/d)\right\}. \tag{36}$$

From the inequalities (31) and (35) it is seen that the distinction between Cases 1 and 2 depends on the relative magnitudes of L/M and l/m. Introducing the values of L, M, l, and m given by (25) and (30) we can write these discriminating inequalities as

$$q\gamma(1-e^2) \gtrless \tfrac{1}{2}ac\phi'(1-e_w^2).$$

Thus, Case 1 applies when collisions between particles and the inclined plane have e_w close to unity and a small value of ϕ'; in other words, when they are almost elastic and almost specular. This would be expected to be the case when the plane is hard and smooth, so we will refer to Case 1 as the 'smooth plane' case. Case 2, on the other hand, corresponds to a value of ϕ' near unity and a small value of e_w; that is, diffuse and highly inelastic collisions between particles and the plane. It will, therefore, be referred to as the 'rough plane' case.

In both cases the total mass flow rate is given by

$$\dot{m} = \rho\int_0^h \frac{u\,\mathrm{d}z}{(1+s/d)^3}, \tag{37}$$

with s given by (21) and u by (33) or (36) for Cases 1 and 2, respectively. Thus

$$\dot{m} = A\frac{\rho t}{qd}\tan\theta\int_0^h \frac{\left\{\int_z^h I_0(W\xi/d)\,\mathrm{d}\xi + \frac{qd}{c\phi'}I_0(Wh/d)\right\}}{\left\{1+\frac{A^2t}{g\cos\theta}\frac{I_0^2(Wz/d)}{z}\right\}^3}\mathrm{d}z \tag{38}$$

for Case 1, and the same expression for Case 2, but with I_0 replaced by J_0 throughout. From this we see that $\dot{m} \propto A$ for small values of A, while $\dot{m} \propto 1/A^5$ for large values of A. It follows that $\dot{m} \to 0$, both as $A \to 0$ and as $A \to \infty$ so, since $\dot{m}$ is bounded and positive for all A, there exists some finite value of A for which $\dot{m}$ is largest. In fact, $\dot{m}$ passes through a single maximum as A increases, and for each value of $\dot{m}$ below this maximum there are two values of A, and hence two solutions. It is easy to show that the flow is slower and denser for the smaller value of A, and faster and less dense for the larger value, though the mass flow rate and the depth of the layer are the same for both solutions. Thus, if we attempt to plot the mass flow rate $\dot{m}$ as a function of the depth h for a plane of given inclination, the high-density collisional theory predicts that we will get a single line of bounded height at a constant value of h (determined by the inclination), and that each point on this line will correspond to two different solutions, in which the same flow rate is achieved by different combinations of velocity and bulk density. This is intuitively disturbing and does not agree with experimental observations, so it appears that the high-density collisional theory is of little value, in itself, for this problem. However, it is instructive to compare it with the predictions of the full collisional theory, of which it is a limiting case.

4. High-density collisional theory, full collisional theory and frictional–collisional theory compared

For the full collisional theory and the frictional–collisional theory solutions must be obtained numerically for specified sets of parameter values. Two cases were considered, corresponding to a 'smooth plane' and a 'rough plane', respectively, as defined in §3. The relevant parameter values are set out in table 1.

Figure 6(*a*) shows the dimensionless mass flow rate ($\dot{m}^* = \dot{m}/\rho_p(gd^3)^{\frac{1}{2}}$), given by the full collisional theory, as a function of the depth of the layer for the case of the smooth plane inclined at an angle of 15°, so that $\tan^2\theta$ lies between l/m and $\tan^2\theta_0$. The curve is seen to start from the origin, rise to a maximum as h/d increases, then decrease again to give zero flow rate at a value of h/d just less than 18. The curve clearly asymptotes to a vertical line as it approaches the h/d-axis, and this is just the unique vertical line predicted by the high-density collisional theory. The reason for this behaviour can be seen from figure 6(*b*), where profiles of solids volume fraction as a function of depth in the layer are shown, corresponding to the points distinguished by circles on the curve of figure 6(*a*). (Here y denotes $h-z$.) As h/d increases, the solids volume fraction profiles are seen to approach ν_0 ($= 0.65$) for all values of y, so the high-density approximation becomes valid. Figures 6(*c*) and 6(*d*), respectively, show profiles of dimensionless velocity, defined by $u^* = u/(gh\sin\theta)^{\frac{1}{2}}$, and dimensionless particle temperature, defined by $T^* = T/gd\cos\theta$. The velocities becomes progressively slower and the particle temperatures progressively smaller as h/d increases, with the last identified point on the curve of figure 6(*a*) corresponding to a thick, 'cold' layer of granular material moving slowly down the plane.

The relation between predictions of the full collisional theory and those of the high-density collisional theory is now plain. The simplifications introduced in the high-density closure cause the curve of mass flow versus depth, found from the full collisional theory, to collapse onto its high-density asymptote, so that it degenerates into a vertical line. The collisional theory predicts that there is a maximum mass flow rate for which fully developed flow is possible, and for each value of the flow rate smaller than this there are two distinct solutions, though we do not know whether

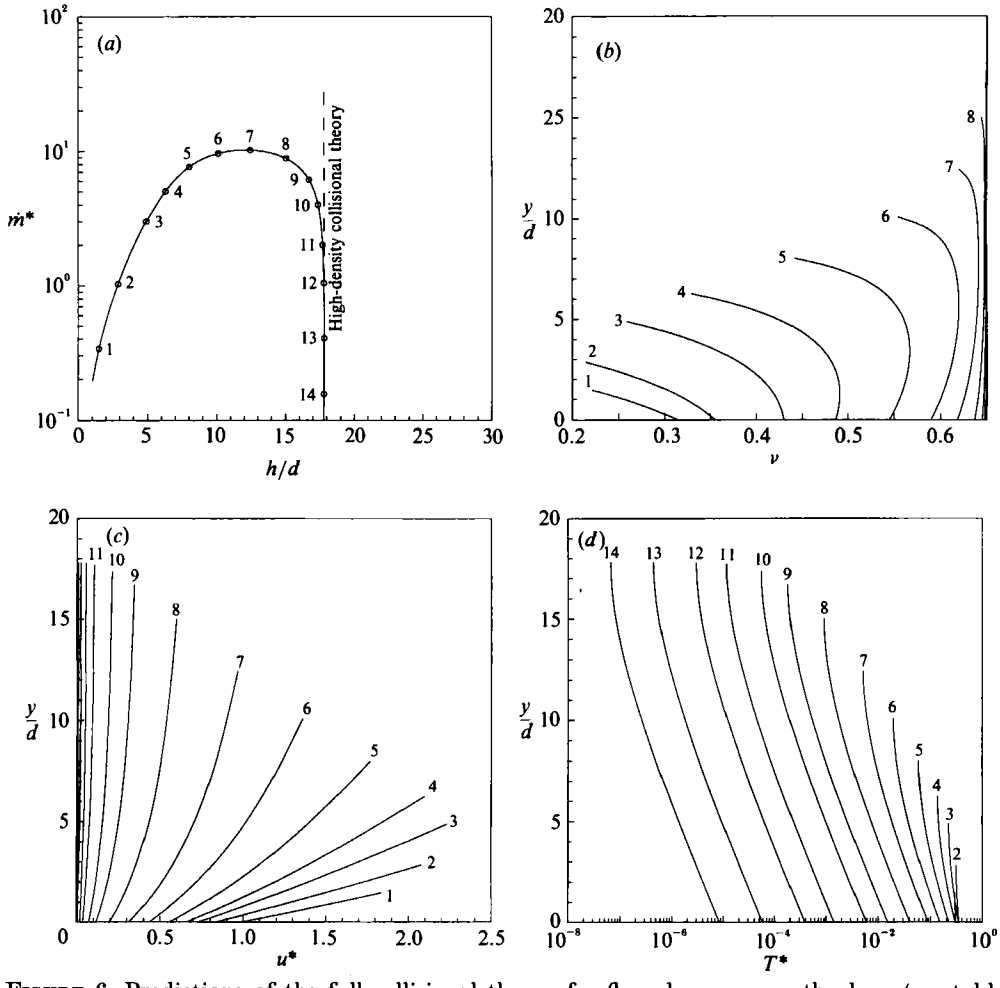

FIGURE 6. Predictions of the full collisional theory for flow down a smooth plane (see table 1) inclined at an angle of 15°. (*a*) Relation between mass flow rate and depth of the flowing layer. (*b*) Profiles of solids volume fraction within the flowing layer. (*c*) Profiles of velocity within the flowing layer. (*d*) Profiles of particle temperature within the flowing layer. Numbers on (*b–d*) correspond to points on (*a*).

Parameter	Smooth plane	Rough plane
e	0.91	0.91
e_w	0.91	0.80
ϕ	28.5°	12.3°
δ	12.3°	28.5°
ϕ'	0.25	0.85
ν_0	0.65	0.65
ρ_p	2.9 g/cm^3	2.9 g/cm^3
d	0.1 cm	0.1 cm
Fr	0.5 g/cm s^2	0.5 g/cm s^2
p	2	2
n	5	5

TABLE 1.

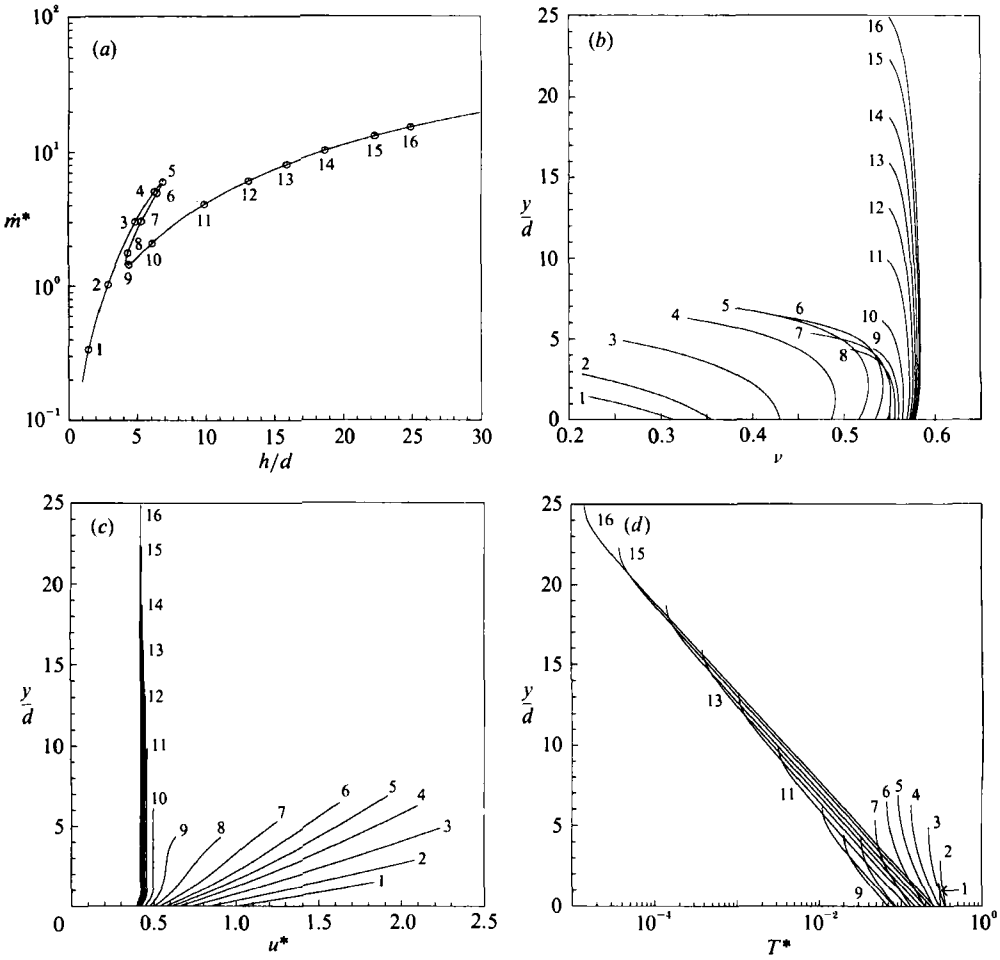

FIGURE 7. Predictions of the frictional–collisional theory for flow down a smooth plane (see table 1) inclined at an angle of 15°. (*a*) Relation between mass flow rate and depth of the flowing layer. (*b*) Profiles of solids volume fraction within the flowing layer. (*c*) Profiles of velocity within the flowing layer. (*d*) Profiles of particle temperature within the flowing layer. Numbers on (*b–d*) correspond to points on (*a*).

both represent stable configurations. Experiments, on the other hand (Johnson *et al.* 1990) usually show a monotonic increase of depth with flow rate over the whole range of flows studied, and no evidence of a multiplicity of the type just described or an upper bound for the depth. Though it is conceivable that behaviour of the type predicted by the collisional theory would be found if the experiments were extended to higher feed rates, there is no evidence of it in the work cited above nor, so far as we know, elsewhere in the literature.

It remains to compare the predictions of the collisional theory with those of the full, frictional–collisional theory for which $\boldsymbol{\sigma} = \boldsymbol{\sigma}_k + \boldsymbol{\sigma}_c + \boldsymbol{\sigma}_f$. The results for this case are shown in figure 7. Comparing figure 7 (*a*) with figure 6(*a*) it is seen that the inclusion of the frictional contribution to the stress has profoundly changed the relation between flow rate and depth. At high flow rates the depth now continues to increase with increasing flow rate: the curve does not dip back to meet the axis $\dot{m}^* = 0$, as in figure 6 (*a*). At the same time there is a new feature, in the form of a maximum and

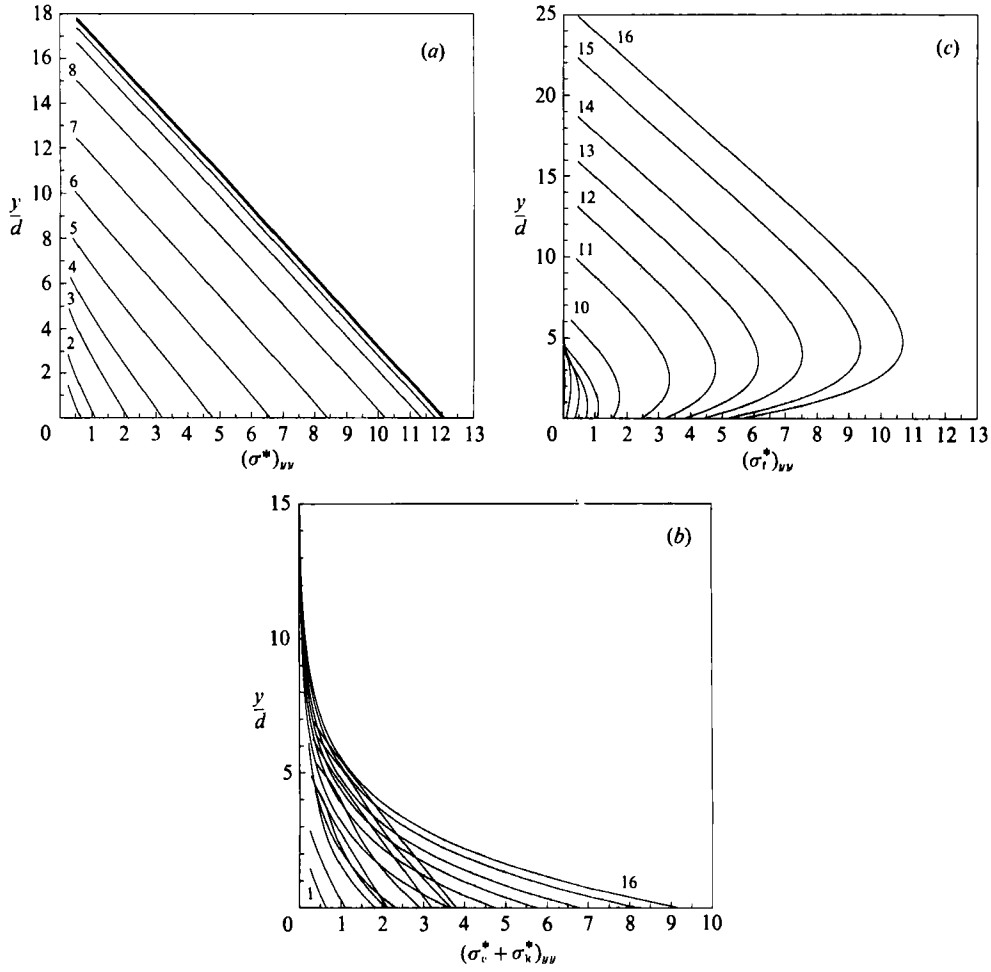

FIGURE 8. Predicted profiles of normal stress within the flowing layer for flow down a smooth plane inclined at 15°. (*a*) From the full collisional theory. (*b*) Sum of collisional and kinetic contributions, from the frictional–collisional theory. (*c*) Frictional contribution, from the frictional–collisional theory. Numbers on (*a*) correspond to points on figure 6(*a*) and those on (*b*, *c*) to figure 7(*a*).

minimum of $\dot{m}^*$ traversed successively by the curve as the depth increases. For values of h below that corresponding to the maximum the curves of figures 6(*a*) and 7(*a*) coincide closely, and comparison of figures 6(*b*) and 7(*b*), 6(*c*) and 7(*c*) and 6(*d*) and 7(*d*) shows that the profiles of volume fraction, velocity, and particle temperature are also in close agreement. Thus, the added frictional terms do not make themselves felt in this interval. Beyond the maximum of $\dot{m}^*$ in figure 7(*a*) the curve diverges sharply from that of figure 6(*a*), and the profiles of volume fraction, velocity, and particle temperature also become quite different for the two cases. The short, descending arc of the curve in figure 7(*a*) represents a sequence of solutions for which there is a rapid transition from flows with smooth velocity profiles, extending throughout the depth of the layer, to a quite different situation in which most of the layer consists of a high-density block of material that slides, without shearing, over a thin shear layer immediately adjacent to the surface of the plane. The transition between the two types of solution is virtually complete by the minimum of the curve in figure 7(*a*). Beyond this point the mass flow rate increases, primarily by adding to

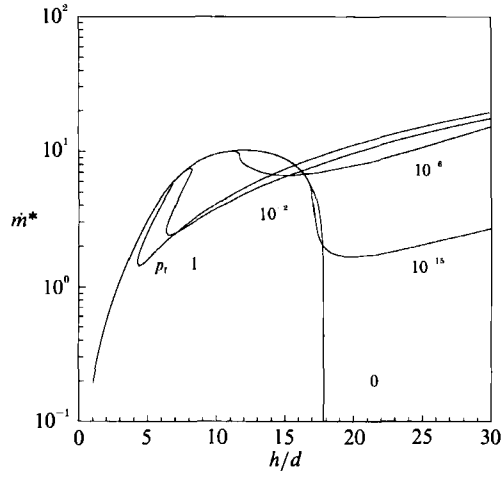

FIGURE 9. The relation between the predictions of the full collisional theory and the frictional–collisional theory, illustrated by the dependence of flow rate on depth for each of these theories, and for three intermediate cases.

the depth of this sliding block without changing its velocity very much, and this process can apparently be continued indefinitely, generating a sustained increase in mass flow rate with the depth of the layer. Despite the fact that the layer is not shearing through most of its depth, figure 7 (*d*) shows that its particle temperature does not vanish, but increases exponentially on moving down from the surface. (Some of the profiles shown in figure 7 are clearly of dubious physical significance; for example, the thinnest layers are little more than one particle diameter in depth, yet substantial variations in velocity and density are shown within the layer. Here and elsewhere we include such results, for what they are worth, as predictions of the continuum theories, leaving aside the important question of whether a continuum description is appropriate in such cases since our purpose is to compare the different continuum theories.)

It is also interesting to compare the stress profiles for the collisional and the frictional–collisional theories. Since the shear stress is simply proportional to the normal stress, through the sine of the angle of friction, it suffices to plot normal stress profiles, and these are shown in figure 8. Figure 8 (*a*) gives the normal stress for the solutions based on the collisional theory: it is seen to build up with increasing depth so as to balance the weight of the overburden of material between the free surface and the point in question. The small deviations from a linear buildup of normal stress with depth reflect the changes in bulk density within the layer. For the frictional–collisional theory figures 8 (*b*) and 8 (*c*) show the contributions from $\sigma_k + \sigma_c$ and from σ_f, respectively, to the total normal stress. At large values of the depth, where most of the layer consists of a sliding block of material of almost constant bulk density, the dominant contribution to the stress is frictional, and it increases linearly with depth, as it must. Near to the inclined plate the frictional contribution to the stress decreases, and it is replaced by an increasing collisional contribution generated by the shearing within the layer of material adjacent to the plate.

The 'switchback' in the curve of figure 7 (*a*) relating mass flow rate and depth should give rise to a hysteresis phenomenon in experiments where the flow rate is controlled, with a sudden increase in depth at the upper end of the switchback as the flow is increased, and a sudden decrease in depth at the lower end as the flow is

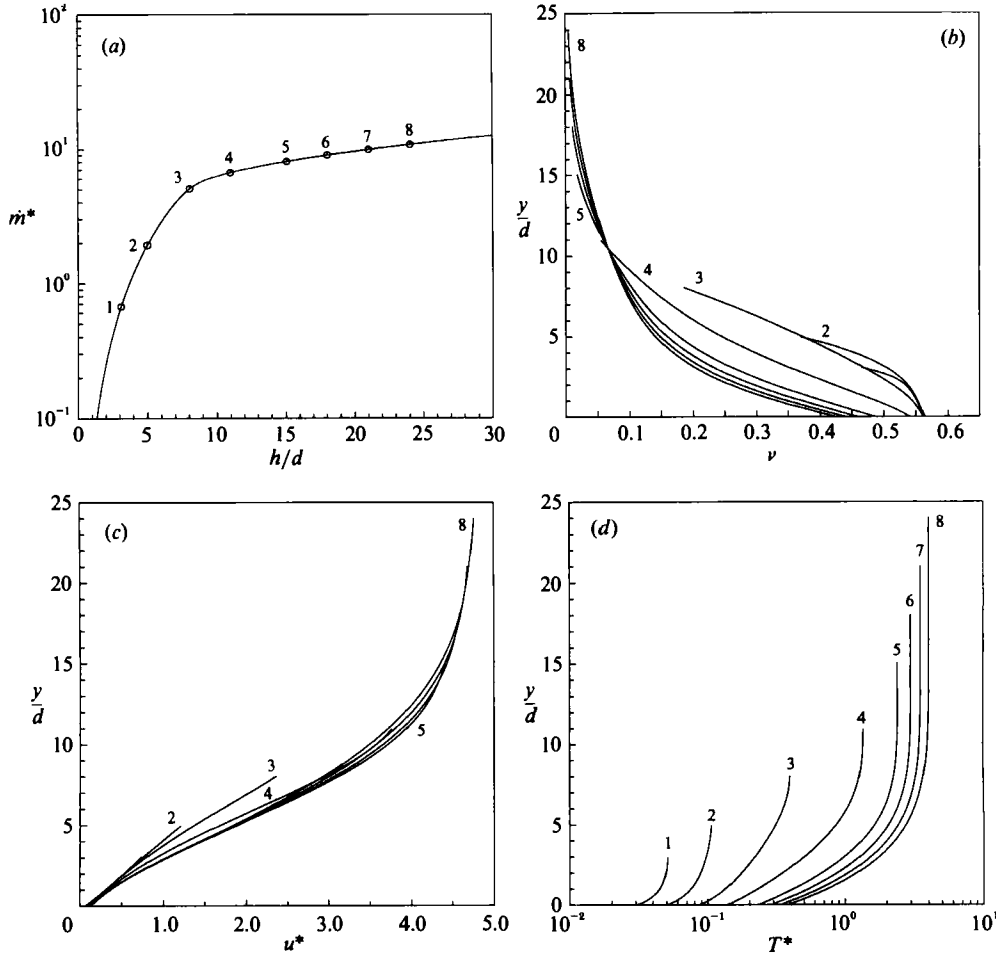

FIGURE 10. Predictions of the frictional–collisional theory for flow down a rough plane (see table 1) inclined at an angle of 19.5°. (*a*) Relation between mass flow rate and depth of the flowing layer. (*b*) Profiles of solids volume fraction within the flowing layer. (*c*) Profiles of velocity within the flowing layer. (*d*) Profiles of particle temperature within the flowing layer. Numbers on (*b–d*) correspond to points on (*a*).

decreased. At least one observation of jumps in depth, which appear to correspond to these predictions, has been reported in the literature (see figure 8 of Johnson *et al.* 1990).

The differences between the predictions of the collisional theory and the frictional–collisional theory are so profound that it is interesting to trace the relation between them through a sequence of intermediate cases. Thus, we can replace σ_f, wherever it appears in the frictional–collisional theory, by $p_f \sigma_f$, where $0 < p_f < 1$. Then $p_f = 0$ gives the collisional theory, $p_f = 1$, gives the frictional–collisional theory, and computed solutions for a sequence of intermediate values of p_f will permit us to elucidate the link between the two. Figure 9 superimposes the computed curves relating $\dot{m}^*$ to h/d for $p_f = 0$, 10^{-15}, 10^{-6}, 10^{-2} and 1, where $p_f = 0$ corresponds to the full collisional theory and $p_f = 1$ to the frictional–collisional theory. At low values of the depth all the curves coincide with the corresponding curve for the collisional theory. As the depth increases, at some point each curve for $p_f \neq 0$ breaks

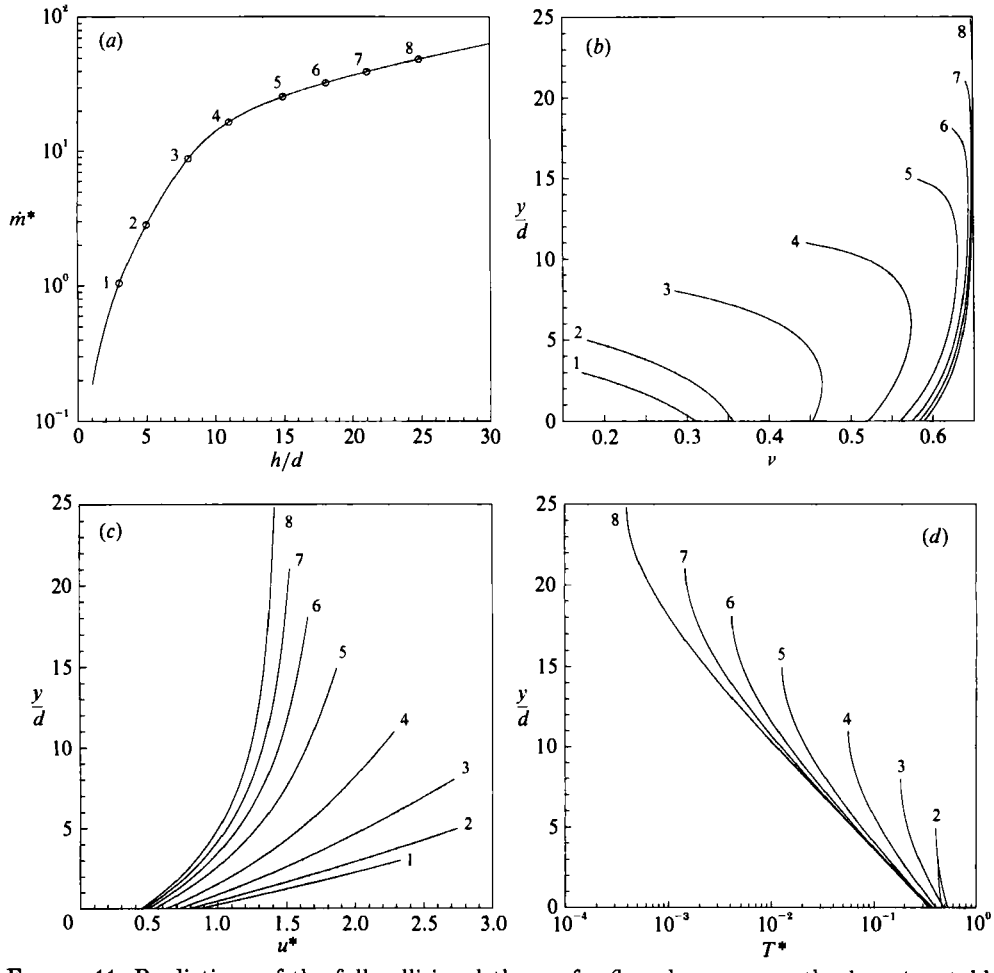

FIGURE 11. Predictions of the full collisional theory for flow down a smooth plane (see table 1) inclined at an angle of 15.5°. (*a*) Relation between mass flow rate and depth of the flowing layer. (*b*) Profiles of solids volume fraction within the flowing layer. (*c*) Profiles of velocity within the flowing layer. (*d*) Profiles of particle temperature within the flowing layer. Numbers on (*b–d*) correspond to points on (*a*).

away from that of the purely collisional theory ($p_f = 0$), dropping first below it, then passing through a minimum and subsequently rising monotonically. For successively increasing values of p_f the point of breakaway occurs at successively smaller values of the depth, converging on figure 7 (*a*) when $p_f \to 1$. However, no matter how small the value of p_f, it appears that the curve for the corresponding frictional–collisional theory always breaks away from the curve for the purely collisional theory before that curve reaches the axis $\dot{m}^* = 0$, after which it rises monotonically as h increases.

All the results presented so far refer to the case of the smooth plane. Figure 10 shows results for the frictional-collisional theory ($p_f = 1$) applied to a rough plane (whose parameter values are listed in table 1) at an inclination of 19.5°. Comparing the profiles of volume fraction, velocity, and particle temperature with those of figure 7 it is seen that the nature of the motion is quite different. Bulk densities are lower, velocities are much higher, and shear now extends much more uniformly through the layer, with comparatively little slip at the surface of the plane. Particle temperatures

are also higher, and the temperature now increases on moving up through the layer, so that the 'hottest' part of the material is adjacent to the free surface, in contrast with the case of the smooth plane, where the 'hottest' material was confined to a narrow region at the bottom of the layer. The overall picture is one of a much looser, more energetic flow, with the plane acting as a sink, rather than a course of pseudo-thermal energy. Figure 10(*a*) shows that the mass flow rate increases monotonically with the depth of the layer, and there is no multiplicity like that seen in figure 6(*a*).

Finally, recall that the high-density collisional theory provided no solutions in the case of a smooth plane with inclination such that $\tan^2\theta_0 < \tan^2\theta < L/M$. Nevertheless, this does not preclude the existence of solutions of the full collisional theory in these circumstances, as seen from figure 11, which shows solutions of the full collisional theory for the smooth plane at an inclination of 15.5°, whose tangent satisfies the above inequalities. In contrast to figure 6(*a*), which corresponds to an inclination of 15°, the curve of $\dot{m}^*$ *vs.* h/d shown in figure 11(*a*) rises monotonically. As h/d increases, the volume fraction profiles of figure 11(*b*) appear to be converging to a limiting profile which does not lie close to ν_0 throughout the depth of the layer, so the solution never approaches a limit that could be derived from the high-density approximation; indeed, as we have seen, that approximation has no solution in this case.

5. Concluding remarks

Available experimental results on flow down inclined chutes indicate that the depth of the flowing layer increases with the flow rate (at least for high values of the flow) to the highest flows investigated. We are not aware of any evidence of a maximum in the curve of flow rate versus depth, such as the collisional theory predicts in the 'smooth plane' results quoted above, nor do there appear to be upper bounds on the flow rate and the depth, as would be the case if the right-hand branch of the predicted curve represented unstable states, and was therefore unrealizable. (The existence of two states for a given flow rate for the case of figure 6(*a*) does not correspond to supercritical and subcritical states of flow, as discussed by Campbell, Brennen & Sabersky (1985). All the states shown in figure 6(*a*) are subcritical, based on the mean velocity.) While the number of experimental investigations is still small, and results from larger chutes at much higher flow rates would be particularly welcome, we can conclude provisionally that the predictions of the collisional theory for the simplest measurable property, namely the relation between layer depth and flow rate, are qualitatively incorrect. The same remarks apply, more emphatically, to the high-density collisional theory of Haff, where the solutions contain inconsistencies with the physical assumptions on which the equations were based, and the predicted relation between flow rate and depth is absurd.

The discrepancies at high flow rates are eliminated when the collisional theory is replaced by the frictional–collisional theory, but at lower flow rates the form of the relation between flow rate and depth may become more complicated. For example, in the 'smooth plane' case investigated here figure 7(*a*) shows that there is an interval of multiplicity in which there are three different values of the depth, and correspondingly three different flow patterns, for each value of the flow rate. Johnson *et al.* (1990) recently reported some observations which are consistent with this prediction, provided the middle branch represents solutions which are unstable, and therefore unobservable. A hysteresis loop would then be traced on increasing and decreasing the flow rate over an interval including the multiplicity, and just such a

hysteresis was reported by the above authors in measurements on a 'smooth base' chute at one particular inclination.

The effect of introducing the 'frictional' terms into the equations cannot be reproduced, even qualitatively, by decreasing the value of the coefficient of restitution in the collisional theory. It is easy to show that this does not change the form of the curve, shown in figure 6(*a*), relating flow to depth, but (for the smooth plane case) it reduces the value of the depth at which the flow rate drops to zero. For the 'rough plane' case, on the other hand, decreasing the coefficient of restitution increases this depth.

It should not be assumed that the shape of the curve in figure 7(*a*) represents the only type of branching behaviour predicted by the frictional–collisional model. Nott & Jackson (1992) have recently shown that more complicated types of behaviour are possible for other values of the parameters, and that the pattern of branching changes radically for quite small changes in these parameters. There has been no extensive exploration of branching behaviour over the parameter space.

Finally, the velocity profiles of figure 7(*c*), predicted by the frictional–collisional model, appear to be consistent with some recent results of direct dynamic simulation of flow of granular material under gravity down a long 'smooth' plane (O. M. Walton 1991, private communication), and the profiles of velocity, volume fraction and temperature for the collisional theory, shown in figure 6, are qualitatively similar to the simulations of Campbell & Brennen (1985).

This work formed part of a programme supported by the National Science Foundation under Grant No. CBT-8504201. The first author also wishes to acknowledge personal support in the form of a National Science Foundation Graduate Fellowship. The second author was a visiting Professor at Rice University while most of the work was in progress. He is grateful for the opportunity this provided for uninterrupted study.

Appendix. Explicit solution for locked flow

The full system of equations governing flow down an inclined plane consists of a set of nonlinear partial differential equations which must be solved using some numerical method. It is practically impossible to extract information about the flowing system without a full solution of the equations. However, there is one limiting case of practical interest for which the pertinent details of the solution may be obtained explicitly; namely the case of 'locked' flow. This is seen in figure 7(*a–d*) for large values of the layer depth, and it is apparent that the volume fraction is approximately constant throughout the layer, while the velocity gradient is non-zero only in a thin sublayer adjacent to the plane surface. Utilizing these two observations, the equations describing the system may be simplified to yield an explicit solution, which can be used as a check for the full solution and to estimate flow rates and other information without the use of a computer.

We begin with the complete frictional–colllisional equations in the notation used by Johnson *et al.* (1990):

$$f_1(\nu)\,T^* + N_f^*(\nu) = A\int_Y^1 \nu\,\mathrm{d}Y + \frac{\pi}{6}\left(\frac{\nu(1)}{\nu_0}\right)^{\frac{2}{3}}, \tag{A 1}$$

$$\frac{f_2(\nu)}{(AB)^{\frac{1}{2}}}\,T^{*\frac{1}{2}}\frac{\mathrm{d}u^*}{\mathrm{d}Y} + \frac{\sin\phi}{B}N_f^*(\nu) = A\int_Y^1 \nu\,\mathrm{d}Y + \frac{\pi}{6}\left(\frac{\nu(1)}{\nu_0}\right)^{\frac{2}{3}}, \tag{A 2}$$

$$f_1(\nu) = 4\nu^2 g_0 \qquad f_6(\nu) = \frac{\pi\sqrt{3\nu g_0}}{4\nu_0 f_3(\nu)}$$

$$f_2(\nu) = \frac{5\pi^{\frac{1}{2}}}{72}\left(\frac{64}{25}+\frac{768}{25\pi}\right)\nu^2 g_0 \qquad f_7(\nu) = \frac{\pi\nu g_0}{2\sqrt{3\nu_0 f_3(\nu)}}$$

$$f_3(\nu) = \frac{25\pi^{\frac{1}{2}}}{128}\left(\frac{144}{25}+\frac{512}{25\pi}\right)\nu^2 g_0 \qquad f_8(\nu) = \frac{\pi\nu g_0}{2\sqrt{3\nu_0 f_2(\nu)}}$$

$$f_5(\nu) = \frac{12}{\pi^{\frac{1}{2}}}(1-e^2)\nu^2 g_0 \qquad g_0 = \frac{1}{1-(\nu/\nu_0)^{\frac{1}{3}}}$$

TABLE 2.

$$\frac{\mathrm{d}}{\mathrm{d}Y}\left[f_3(\nu)T^{*\frac{1}{2}}\frac{\mathrm{d}T^*}{\mathrm{d}Y}\right]+ABf_2(\nu)\,T^{*\frac{1}{2}}\left(\frac{\mathrm{d}u^*}{\mathrm{d}Y}\right)^2-A^2f_5(\nu)\,T^{*\frac{3}{2}}=0. \tag{A 3}$$

The first two equations are the integrated form of the momentum equations, while the third is the pseudo-thermal energy balance (equation (3)) in the present paper, with a term in $\mathrm{d}\nu/dY$ neglected (Johnson *et al.* 1990). The remaining boundary condition at the free surface ($Y = 1$) is simply

$$\frac{\mathrm{d}T^*}{\mathrm{d}Y} = 0, \tag{A 4}$$

while the conditions at the plane surface ($Y = 0$) take the form

$$\frac{f_2(\nu)}{(AB)^{\frac{1}{2}}}T^{*\frac{1}{2}}\frac{\mathrm{d}u^*}{\mathrm{d}Y}+\frac{\sin\phi}{B}N_{\mathrm{f}}^*(\nu) = \left(\frac{A}{B}\right)^{\frac{1}{2}}Df_2(\nu)f_8(\nu)\,T^{*\frac{1}{2}}u_{\mathrm{sl}}^*+\frac{\tan\delta}{B}N_{\mathrm{f}}^*(\nu), \tag{A 5}$$

$$\frac{\mathrm{d}T^*}{\mathrm{d}Y} = ACf_6(\nu)\,T^*-A^2BDf_7(\nu)\,u_{\mathrm{sl}}^{*2}. \tag{A 6}$$

The functions f_1–f_8 are given in table 2. We use a simplified form of these functions, differing from those used by Johnson *et al.* in that the forms given here hold for $g_0 \gg 1$, which is indeed the case for dense 'locked' flows. This assumption breaks down only for very low-density flows of the sort not considered here. The dimensionless spatial coordinate, Y, and frictional normal stress, N_{f}^*, are defined by

$$Y = \frac{y}{h}, \quad N_{\mathrm{f}}^*(\nu) = \frac{N_{\mathrm{f}}(\nu)}{\rho_{\mathrm{p}} g d\cos\theta} \tag{A 7}$$

and the dimensionless parameters A, B, C, and D are given by

$$A = h/d, \quad B = \tan\theta, \quad C = (1-e_{\mathrm{w}}^2), \quad D = \phi'. \tag{A 8}$$

With the system thus defined, we take advantage of the facts that the solids volume fraction, ν, is roughly constant and that the velocity gradient is zero in the bulk of the flow to reduce (A 2) and (A 3) to the form

$$\frac{\sin\phi}{B}N_{\mathrm{f}}^*(\nu) = A\int_Y^1 \nu\,\mathrm{d}Y+\frac{\pi}{6}\left(\frac{\nu(1)}{\nu_0}\right)^{\frac{2}{3}}, \tag{A 9}$$

$$f_3(\nu)\frac{\mathrm{d}}{\mathrm{d}Y}\left[T^{*\frac{1}{2}}\frac{\mathrm{d}T^*}{\mathrm{d}Y}\right]-A^2f_5(\nu)\,T^{*\frac{3}{2}}=0. \tag{A 10}$$

Equation (A 10) may then be solved directly to give the particle temperature profile:

$$T^{*\frac{3}{2}} = T_0^{*\frac{3}{2}} \exp(-\lambda Y)\left\{\frac{1+\exp[-2\lambda(1-Y)]}{1+\exp[-2\lambda]}\right\}, \tag{A 11}$$

where

$$\lambda = A\left(\frac{3f_5(\nu)}{2f_3(\nu)}\right)^{\frac{1}{2}}, \tag{A 12}$$

and where T_0^* is the dimensionless particle temperature at the plane surface. The term in braces in (A 11) is only significant close to the free surface and may be neglected in the lower two thirds of the flowing material, yielding the simple exponential profile

$$T^* = T_0^* \exp(-\tfrac{2}{3}\lambda Y). \tag{A 13}$$

From the full solutions shown in figure 7(*d*) it is apparent that this exponential solution is valid even where the velocity gradient is non-zero near the surface of the chute. Based on this observation, we then use the grain-temperature profile from (A 13) in (A 5) and (A 6) to find the particle temperature and the slip-velocity at the base of the plane:

$$u_{\mathrm{sl}}^* = \left(\frac{ACf_6(\nu)+\frac{2}{3}\lambda}{A^2BDf_2(\nu)}\right)^{\frac{1}{2}} T_0^{*\frac{1}{2}}, \tag{A 14}$$

$$T_0^* = (B-\tan\delta)\left[A\nu+\frac{\pi}{6}\left(\frac{\nu}{\nu_0}\right)^{\frac{2}{3}}\right]\left\{\left(\frac{D}{A}\right)^{\frac{1}{2}}\frac{f_2(\nu)f_8(\nu)}{[f_7(\nu)]^{\frac{1}{2}}}[ACf_6(\nu)+\tfrac{2}{3}\lambda]^{\frac{1}{2}}-f_1(\nu)\tan\delta\right\}^{-1}, \tag{A 15}$$

where we have used the fact that

$$\int_Y^1 \nu\,\mathrm{d}Y \approx \nu(1-Y). \tag{A 16}$$

It is then possible to use the full form of the momentum equations near the plane surface to obtain the velocity gradient in the region near $Y = 0$:

$$\frac{f_2(\nu)}{(AB)^{\frac{1}{2}}} T^{*\frac{1}{2}} \frac{\mathrm{d}u^*}{\mathrm{d}Y} = \left[A\nu(1-Y)+\frac{\pi}{6}\left(\frac{\nu}{\nu_0}\right)^{\frac{2}{3}}\right]\left(1-\frac{\sin\phi}{B}\right)+\frac{\sin\phi}{B}f_1(\nu)\,T^*. \tag{A 17}$$

By using (A 17) and (A 13) we may then calculate the position Y_{L} at which the flowing material 'locks' and the velocity gradient becomes zero. The result is a nonlinear equation which may easily be solved by successive substitution when written in the form

$$-\tfrac{2}{3}\lambda Y_{\mathrm{L}} = \ln\left(1-\frac{B}{\sin\phi}\right)+\ln\left[A\nu(1-Y_{\mathrm{L}})+\frac{\pi}{6}\left(\frac{\nu}{\nu_0}\right)^{\frac{2}{3}}\right]-\ln[f_1(\nu)\,T_0^*]. \tag{A 18}$$

It is then straightforward to integrate (A 17) from $Y = 0$ to Y_{L} to obtain the velocity u_{L} in the bulk of the material

$$\begin{aligned} u_{\mathrm{L}}^* - u_{\mathrm{sl}}^* = \frac{3(AB)^{\frac{1}{2}}}{\lambda f_2(\nu)}\Bigg\{&\left(\frac{\sin\phi}{B}-1\right)\left[A\nu(1-Y)+\frac{\pi}{6}\left(\frac{\nu}{\nu_0}\right)^{\frac{2}{3}}\right][T_0^{*-\frac{1}{2}}-T_{\mathrm{L}}^{*-\frac{1}{2}}] \\ &+\left(\frac{\sin\phi}{B}-1\right)A\nu Y_{\mathrm{L}}\,T_{\mathrm{L}}^{*-\frac{1}{2}}+\frac{\sin\phi}{B}f_1(\nu)[T_0^{*\frac{1}{2}}-T_{\mathrm{L}}^{*\frac{1}{2}}] \\ &+\left(\frac{\sin\phi}{B}-1\right)A\nu\left(\frac{3}{\lambda}\right)[T_0^{*-\frac{1}{2}}-T_{\mathrm{L}}^{*-\frac{1}{2}}]\Bigg\}, \end{aligned} \tag{A 19}$$

Quantity	Numerical solution	Explicit solution
ν	0.567	0.566
T_0^*	0.1192	0.1195
u_{si}^*	0.4256	0.4236
Y_L	~0.07	0.0744
u_L^*	0.4601	0.4445
$\dot{m}^*$	4.058	3.980

TABLE 3.

where

$$T_L^* = T_0^* \exp(-\tfrac{2}{3}\lambda Y_L).$$

The mass flow rate may then be computed either by considering all of the material to be moving with velocity u_L or by using a simple trapezoidal formula to integrate the layer between $Y = 0$ and Y_L. The error in using the former method over the latter is less than 1%. Thus a simple calculation gives the flow rate of the moving material:

$$\dot{m}^* = \frac{\dot{m}}{\rho_p (gd^3)^{\frac{1}{2}}} = A^{\frac{3}{2}} (\sin\theta)^{\frac{1}{2}} \nu u_L^*. \tag{A 20}$$

All of the results above are based on the assumption that the solids volume fraction, ν, is known. Thus, it remains only to estimate ν to calculate all the important characteristics of the 'locked' flow. This estimate must be made using the one piece of information that has not yet been utilized; that is, the functional dependence of the normal stress on the volume fraction. We could use either of the momentum equations to solve for ν, but it is easier to use the form (A 9) which involves only the volume fraction and the normal stress. We take the expression for the normal stress used by Johnson *et al.* (1990):

$$N_i^*(\nu) = \frac{Fr^*}{\cos\theta} \frac{(\nu - \nu_{min})^2}{(\nu_0 - \nu)^5}, \tag{A 21a}$$

where

$$Fr^* = Fr/(\rho_p g d). \tag{A 21b}$$

It is necessary to choose a value of Y at which to solve (A 9). For the present, we have chosen to integrate this equation over the entire layer to calculate an 'average' value of ν. The resulting nonlinear equation may again be arranged in a form which is easily solved by successive substitution:

$$\nu = \nu_0 - \left\{ \frac{\sin\phi}{\sin\theta} \frac{Fr^*(\nu - \nu_{min})^2}{[\frac{1}{2}A\nu + \frac{1}{6}\pi(\nu/\nu_0)^{\frac{2}{3}}]} \right\}^{\frac{1}{5}}. \tag{A 22}$$

With the volume fraction then known, all of the other quantities may be calculated.

Finally, to illustrate the accuracy of this explicit solution, we compare the results of these calculations with one of the full numerical solutions shown in figure 7(*a–d*), that corresponding to a depth $h/d = 9.89$. The important quantities are compared in table 3 and the particle temperature profiles given by (A 11) and (A 13) are compared to the exact solution in figure 12. It is apparent from table 3 that even the quantities

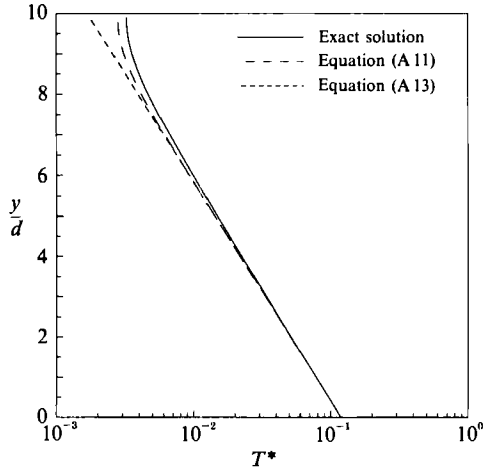

FIGURE 12. Particle temperature profile calculated from the frictional–collisional theory for a layer with $h/d = 9.89$ flowing down the smooth plane at an inclination of 15°, compared with approximate profiles obtained from equations (A 11) and (A 13), respectively.

that differ most from the full numerical solution do so by less than 5%. Likewise, the simple particle temperature distributions given by (A 11) and (A 13) give a good representation of the actual particle temperature profile. Based on comparisons such as these, we may be satisfied with the validity of the approximations made in deriving this explicit solution. This approximate solution is valid for flows in which the density of the bed is high and nearly uniform. It is hoped that the solution given here will make the theory more tractable for 'locked' flows since it removes the need for computer solutions in determining important characteristics of the system.

REFERENCES

CAMPBELL, C. S. 1990 Rapid granular flows. *Ann. Rev. Fluid Mech.* **22**, 57–92.

CAMPBELL, C. S. & BRENNEN, C. E. 1985 Chute flows of granular material: some computer simulations. *Trans. ASME* E: *J. Appl. Mech.* **52**, 172–178.

CAMPBELL, C. S., BRENNEN, C. E. & SABERSKY, R. H. 1985 Flow regimes in open-channel flows of granular materials. *Powder Tech.* **41**, 77–82.

HAFF, P. K. 1983 Grain flow as a fluid mechanical phenomenon. *J. Fluid Mech.* **134**, 401–430.

JOHNSON, P. C. & JACKSON, R. 1987 Frictional–collisional constitutive relations for granular materials, with applications to plane shearing. *J. Fluid Mech.* **176**, 67–93.

JOHNSON, P. C., NOTT, P. & JACKSON, R. 1990 Frictional–collisional equations of motion for particulate flows and their applications to chutes. *J. Fluid Mech.* **210**, 501–535.

LUN, C. K. K., SAVAGE, S. B., JEFFREY, D. J. & CHEPURNIY, N. 1984 Kinetic theories for granular flow: inelastic particles in Couette flow and slightly inelastic particles in a general flow field. *J. Fluid Mech.* **140**, 223–256.

NOTT, P. & JACKSON, R. 1992 Frictional–collisional equations of motion for granular materials and their application to flow in aerated chutes. *J. Fluid Mech.* **241**, 125–144

SAVAGE, S. B. 1983 Granular flows down rough inclines – review and extension. In *Proc. US–Japan Seminar on New Models and Constitutive Relations in the Mechanics of Granular Materials* (ed. J. T. Jenkins & M. Satake). Elsevier.